Bulletin of the Seismological Society of America, Vol. 81, No. 1, pp. 139-161, February 1991

LATE QUATERNARY FAULTING AND THERMOLUMINESCENCE DATING OF THE EAST CACHE FAULT ZONE, NORTH-CENTRAL UTAH

BY JAMES MCCALPIN AND S. L. FORMAN

ABSTRACT

The East Cache fault zone (ECFZ), the southernmost of five en-echelon Quaternary normal faults between the Wasatch and Teton faults, displays evidence of two large paleoearthquakes in the last 15,000 years (15 ka). Stratigraphic data from a trench on the central segment of the ECFZ are augmented with one radiocarbon date, the regional radiocarbon chronology, and 14 thermoluminescence (TL) age estimates. Of the 14 TL analyses performed by Alpha Analytic Inc., only 8 satisfied our criteria for statistical acceptability (< 20 per cent coefficient of variation, < 50 per cent extrapolation to residual TL level). The TL age estimates broadly bracket the earlier faulting event at between 8.7 ± 1.0 and 17.4 ± 3.0 ka, and the later event at between 2.5 ± 0.5 and 8.7 ± 1.0 ka. One radiocarbon age further constrains the earlier event to be younger than 15,540 ± 130 yr BP. Correlation of local Quaternary deposits to the regional radiocarbon chronology provides indirect, but more tightly limiting, age constraints of ca. 4 to ca. 7 ka for the later event, and ca. 13 ka to 15,540 ± 130 yr BP for the earlier event. Both events had small vertical displacements at the trench site (0.8 to 1.8 m), but the cumulative net vertical tectonic displacement elsewhere is up to 4.2 m, suggestive of M_s 6.9 to 7.1 paleoearthquakes. Single-event displacements and the extent of fault scarps suggest that these two paleoearthquake ruptures were probably limited to the 20-km-long central segment of the East Cache fault zone near Logan, Utah. The elapsed time since the most recent event on the central segment (ca. 4 to ca. 7 ka) is somewhat less than the estimated recurrence interval between the latest two paleoearthquake (8.6 ± 3.0 ka). However, comparison of only a single poorly constrained recurrence interval with the elapsed time does not result in a confident assessment of future earthquake potential.

INTRODUCTION

The purpose of this study was twofold: (1) to define the late Quaternary history of the East Cache fault zone (ECFZ) to augment the historic seismic record for assessing local earthquake hazard and (2) to compare the paleoseismic chronology of the ECFZ with those of its neighboring faults. Our study paralleled contemporaneous paleoseismic studies of the adjacent Wasatch fault zone by the USGS (Machette *et al.*, 1987).

The 77-km-long East Cache fault zone (originally termed the Bear River Range fault by Bailey, 1927) is a major west-dipping Neogene normal fault that separates Cache Valley from the Bear River Range in north-central Utah (Fig. 1). Seismic reflection data show that the East Cache fault dips west under Cache Valley at roughly 60° near the surface, flattening to 45° to 55° at depths of 3.5 to 4.0 km (Smith and Bruhn, 1984) and probably cuts the Sevier-age Paris thrust (Evans and Oaks, 1990). Tertiary basin-fill deposits, up to 3.5-km thick

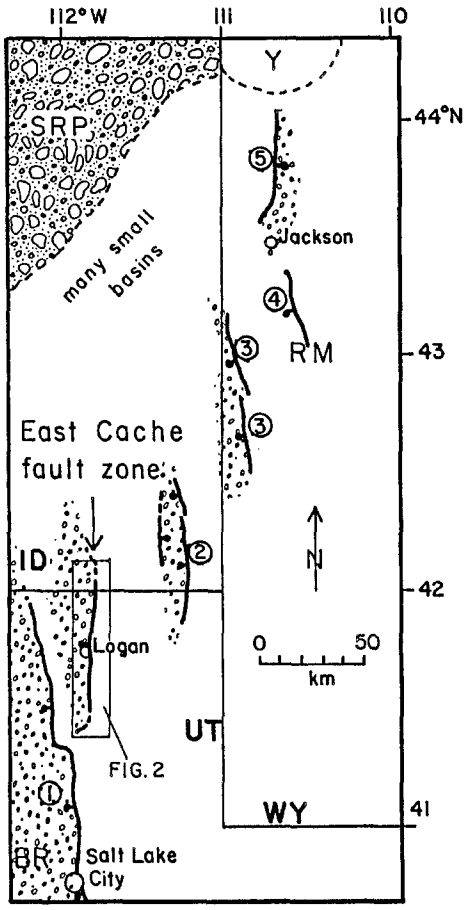

FIG. 1. Location map of the East Cache fault zone in Utah (UT) and Idaho (ID), showing its regional relation to other faults having major late Cenozoic displacement in these states and Wyoming (WY). 1: Wasatch fault zone; 2: Bear Lake faults; 3: Star Valley fault; 4: Hoback fault; 5: Teton fault. SRP: Snake River Plain; Y: Yellowstone volcanic complex; BR: Basin and Range Province; RM: Rocky Mountains. Box shows area of Figure 2. Patterned areas show major intermontane basins formed by Cenozoic faulting and the Snake River Plain.

near Logan, dip gently eastward into the ECFZ. Based on gravity data, Zoback (1983) suggests the Neogene basin fill is as much as 4-km thick near Hyrum, Utah (Fig. 2), which implies a total Neogene throw of at least 4.5 km for the ECFZ (Evans and Oaks, 1990).

The ECFZ is the southernmost of five major Neogene normal faults that form a northeast-trending belt extending from the northern part of the Wasatch fault zone to the Yellowstone volcanic complex (Fig. 1). This belt of right-stepping en-echelon faults marks the boundary between the Basin and Range and the Rocky Mountain structural provinces and is informally termed the Northern Wasatch to Teton Corridor (NWTC). The chronology of late Quaternary faulting on NWTC faults has been studied in reconnaissance for most faults (East Cache fault zone: Swan *et al.*, 1983; McCalpin, 1987a; James Peak fault: Nelson and Sullivan, 1987; Bear Lake faults: Robertson, 1978; McCalpin *et al.*, 1990a; Star Valley fault: Piety *et al.*, 1986; McCalpin *et al.*, 1990b; Teton fault: Gilbert *et al.*, 1986; Byrd and Smith, 1990). However, few of these studies have provided

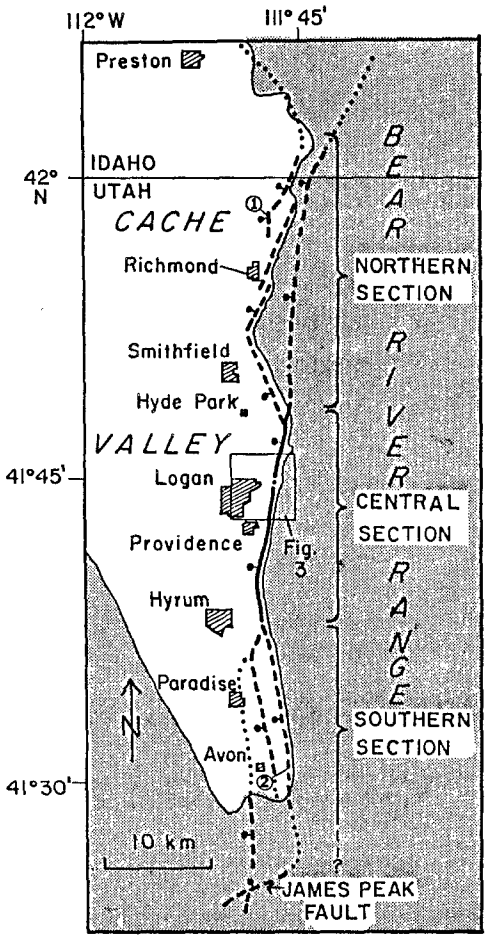

FIG. 2. Map of East Cache fault zone (ECFZ) showing the main fault trace at base of Bear River Range, the three sections, and the James Peak fault at the southern end of Cache Valley. Faults are shown by a heavy solid line where deposits of the Bonneville Lake Cycle (or younger) are displaced, by a dashed line where only pre-Bonneville Quaternary deposits are displaced, and by a dotted line where inferred. Box shows area of Figure 3. Locations of natural exposures (1 and 2) mentioned in the text are shown.

radiometric age control on any individual late Quaternary paleoearthquakes. In this paper, we provide quantitative constraints on the ages of the latest two paleoearthquakes on the ECFZ. We obtained one radiocarbon age and eight thermoluminescence age estimates on faulted Quaternary deposits from a trench excavated across the central segment of the ECFZ. These age determinations generally confirm the ages of faulting inferred by Swan *et al.* (1983) from geomorphic evidence and regional radiocarbon chronology.

GEOMETRY OF THE ECFZ

We divide the ECFZ into three sections (northern, central, and southern) based on fault zone complexity, tectonic geomorphology, and expression of surface fault scarps (Fig. 2). The northern section (at least 33 km long) is characterized by two to three parallel fault traces, by three or four sets of spur facets at the range front, and by a lack of fault scarps in late Pleistocene and

younger deposits (McCalpin, 1989). The 20 km-long central section is defined by a single fault trace, a steep range front with seven recognizable facet sets, and fault scarps displacing deltas of late Pleistocene Lake Bonneville. The 24-km-long southern section is similar to the northern section and contains three parallel fault traces, four sets of range front facets, and fault scarps only in middle Pleistocene(?) or older deposits. At the extreme southern end of Cache Valley, the James Peak fault (Nelson and Sullivan, 1987) may be a southward extension of the southern section. However, the James Peak fault trends nearly perpendicular to the rest of the ECFZ, and fault scarps cannot be continuously traced between the James Peak fault and the southern section as defined in this paper (Cluff *et al.*, 1974; McCalpin, 1989). We present evidence later that the central section is also a seismogenic segment, but that its boundaries with adjacent fault segments may be nonpersistent (cf. Wheeler and Krystinik, 1988).

Trench Stratigraphy on the Central Segment

Geomorphic Setting

Deposits along the East Cache fault zone are predominantly nearshore gravels and sands deposited during the Bonneville lake cycle (13 to 30 ka; Scott *et al.*, 1983). Lacustrine deposits can be associated with either the Bonneville highstand (1565 m elevation here, age 14.5 to 17 ka, Currey and Oviatt, 1985; map unit lbs in Fig. 3) or the Provo shoreline of the regressive phase (1475 m elevation, age ca. 13 ka, Currey and Oviatt, 1985; map unit lpg in Fig. 3). Holocene alluvial fans of two ages (map units af_1, and af_2, Fig. 3) were subsequently deposited near canyon mouths and bury much of the lacustrine deposits along the fault zone.

West-facing fault scarps representing 1.4 to 4.2 m of vertical surface offset are preserved along the northern 8 km of the 20-km-long central segment (Figs. 2 and 3). Scarps displacing the Provo-level delta and a post-Provo strath terrace north of Logan Canyon exhibit surface offsets of 1.2 to 1.4 m, while scarps displacing the older Bonneville highstand deposits south of Logan Canyon display offsets of 2.2 to 4.2 m. Holocene alluvial fans are not displaced. Swan *et al.* (1983) used these geomorphic relationships to infer that two paleoearthquakes had occurred subsequent to the Bonneville highstand, but neither event was radiometrically dated due to lack of datable material.

We trenched a 6.3-m-high fault scarp having 2.5 m of vertical surface offset on the Bonneville highstand delta surface (Fig. 3) to confirm the number of paleoearthquakes recorded in this scarp and to obtain datable material to constrain fault timing. The site was selected because of: (1) good preservation of the suspected two-event scarp, (2) the low-gradient of unmodified depositional surfaces above and below the scarp, and (3) ease of access. Landslide head scarps exist parallel to and west of the trench site (Swan *et al.*, 1983) but can be distinguished from fault scarps by their discontinuous nature and coincidence with hummocky landslide topography. The trench was 65 m long, 1 m wide, and up to 3.5 m deep, and it exposed both Bonneville lake cycle deposits and younger scarp-derived colluvium.

Trench Stratigraphy and Structure

Sediments exposed in the Logan trench were subdivided into seven major units based on differences in grain size, sedimentary structures, and structural

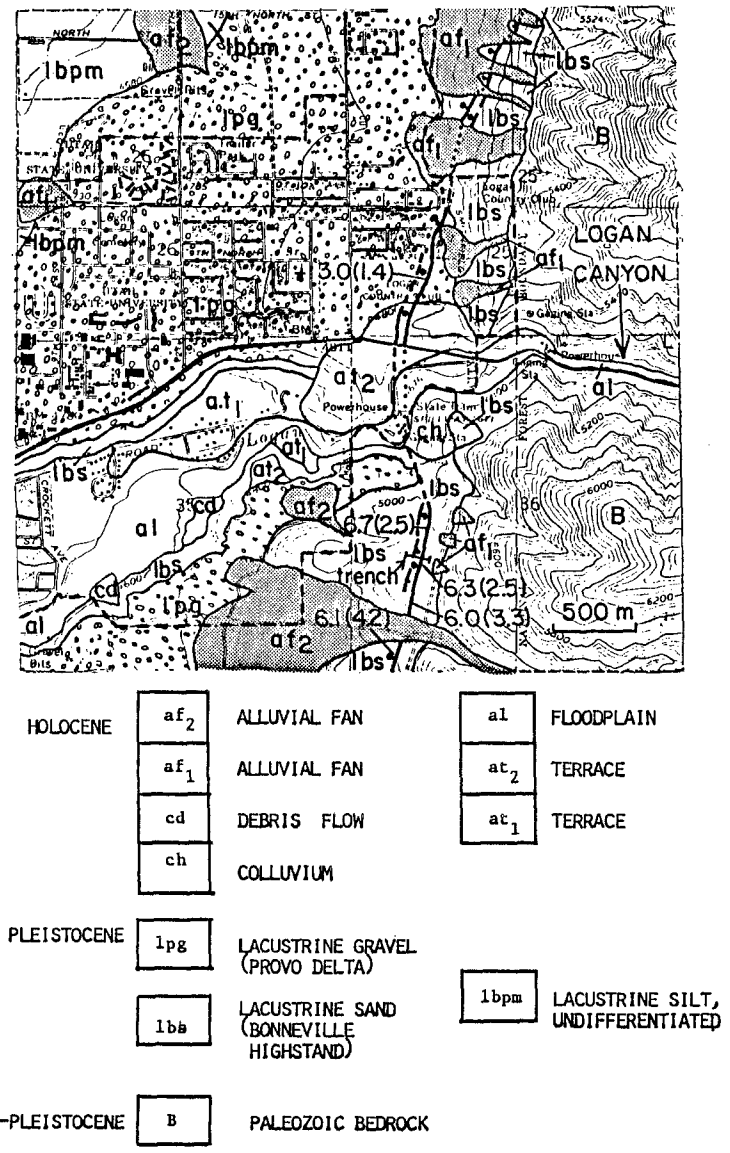

FIG. 3. Geologic map of the area near the mouth of Logan Canyon, Logan, Utah, after McCalpin (1989). Present city limits of Logan, Utah, are demarcated by heavy dashes. Well-preserved fault scarps are shown by heavy solid line, with bar and ball on downthrown side. Scarp height (m) and vertical surface offset (m; in parentheses) shown at selected locations. Heavy dashed line indicates poorly preserved scarp; heavy dotted line indicates fault is concealed. Site of the Logan trench south of the Logan River (in map unit lbs) is shown. Base map from the Logan, Utah, and Smithfield, Utah, 7 1/2′ quadrangles; contour interval 40 feet; elevations in feet above sea level.

relations to fault planes (Fig. 4 and Table 1). The two oldest units (1 and 2) are well-sorted, horizontally stratified medium sands of shallow lacustrine origin. A thin, well-sorted sandy marker bed in unit 1 (thin black bed in Fig. 4b) can be correlated across the several faults in the upthrown block, but cannot be observed in the downthrown block. Its absence in unit 2 suggests that these two units may be the same deposit offset by the main fault trace but exposed at different stratigraphic levels. Units 3a and 3b are cross-bedded gravels of

shallow lacustrine origin that dip eastward on the upthrown side and westward on the downthrown side of the main fault, respectively. Unit 4 is a complex melange of convoluted sand, sand blows, and intact sand blocks (probably pieces of unit 1). Unit 5 is a thin sandy gravel which forms a transition unit between units 3b and 7 on the downthrown fault block. Unit 6 is a thick, massive silt with the downslope tapering wedge shape of a scarp-derived colluvial wedge. The scarp is mantled by about 0.75 m of poorly sorted gravelly slopewash and colluvium (unit 7).

Displacement occurs on six major faults (lettered A through F, Fig. 4c) that dip westward at 65° to 75° near the trench floor and steepen to nearly vertical near the surface. Total vertical stratigraphic displacement of 4.3 m is measured by projecting the top of lacustrine gravels upslope of the scarp downslope over the faulted gravels of the downthrown block. Several small antithetic faults dip eastward at 55° to 75° and have vertical displacements of up to 10 cm. Massive sand was evidently mobilized upwards along faults A and B to form sand-blow-like features (Fig. 4c). The 80-cm-wide zone between the upper parts of faults E and F is filled with displaced chunks of silt and sand in a matrix of deformed sand, and may represent a tension crack fill. Cross-cutting relationships and differential displacements of the marker bed versus the major unconformity (heavy wavy line, Fig. 4c) allow displacements on some of the six major faults to be partitioned between the earlier and later faulting events (see displacement values underneath each fault in Fig. 4c). The method for differentiating these displacements is explained in the caption of Fig. 4, while the implications are discussed in the section called Chronology of Faulting. Some 27 m downslope from the main fault zone a narrow antithetic fault zone exhibits 0.8 m of vertical stratigraphic displacement in unit 3b, but only creates a weak inflection of the ground surface (Figs. 4a and b).

Radiometric and Numerical Ages of Trench Units

Radiocarbon Ages

Only a single sample suitable for radiocarbon dating was retrieved from the trench. Gastropod shells from unit 3b yielded an accelerator mass spectrometry radiocarbon age of 15,540 ± 130 yr BP (AA-4017). This age correlates well with other radiocarbon ages from Bonneville highstand deposits, which range from 15.4 to 16.1 ka (Currey and Oviatt, 1985, Table 1). However, this radiocarbon date only provides a maximum limiting age for the earlier of the two faulting events, whereas we sought bracketing radiometric ages for both events exposed in the trench.

Thermoluminescence Age Estimates

The presence of fine-sandy lacustrine deposits and loess-rich colluvium in the trench suggested that thermoluminescence (TL) dating might be useful in dating the inorganic units. Previous work had shown that shallow marine sands (Forman *et al.*, 1987; Forman, 1989) and loess (Wintle and Huntley, 1982; Rendell and Townsend, 1988) both yielded accurate TL age estimates. We collected 12 TL samples from the Logan trench and two samples from an exposure in the southern fault segment. Sample collection methods are described in Appendix 1.

Briefly, the TL technique estimates the time that sediments have been buried

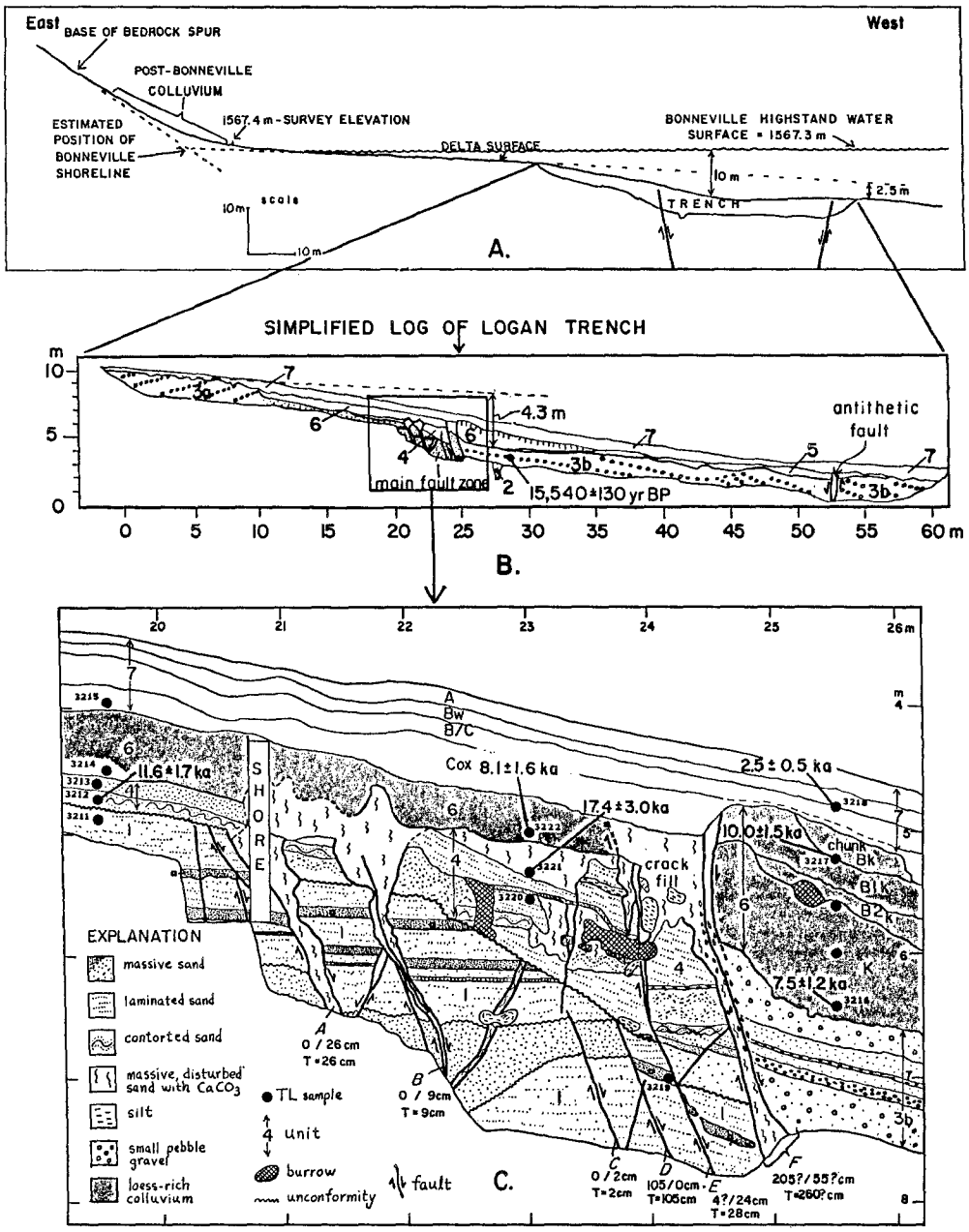

FIG. 4. Cross section showing (a) the geomorphic position of the Logan trench and its relation to the Bonneville shoreline; (b) a simplified log of the trench; and (c) a detailed log of the middle portion of the trench. The trenched fault scarp about 100 m west of the Bonneville shoreline has a net vertical tectonic displacement of 2.5 m. Lacustrine sediments exposed in the trench were deposited in 3 to 10 m of water. (b) Bold numbers refer to units of Table 1. Open circles: pebble gravel; stipples: sand; solid black bed in sand: marker bed used to determine total stratigraphic displacement (see (c)). Box shows area of Figure 4C. Six major faults (heavy lines, lettered A through F) contribute to displacement in the main fault zone. Below letters, numbers before and after slash are vertical displacements (in cm) during the earlier and later faulting events, respectively. T = total vertical displacement (in cm). Total vertical displacement was measured based on offsets of a sandy marker bed (a); displacement during the later event was measured based on offsets of the major unconformity (heavy wavy line) underlying unit 4 (the post-earlier event tectonic "melange"). Displacement inferred for the earlier event is the difference between total displacement and displacement due to the later event. Numbered black circles show TL samples and age estimates, which correlate with Tables 2, 3, and 4; unnumbered circles indicate samples collected but not analyzed.

TABLE 1

DEPOSITIONAL CHARACTERISTICS OF LOGAN TRENCH DEPOSITS

Lithofacies*	Lithology	Environment of Deposition	Dominant Deposition Process	Inferred Degree of Sunlight Exposure†
1, 2	Medium sand	Nearshore lake	Traction and suspended load in littoral zone (< 5 m water depth)	High
3a, b	Pebble gravel	Nearshore lake	Traction load in littoral zone (< 2–3 m water depth)	High
4	Medium sand	Slope of fault scarp	Rapidly deposited gravity-fall, sliding, and rolling blocks from fault scarp free face; liquefied sand injected from beneath	Very low
5	Sandy gravel	Footslope of scarp	Rapidly deposited thin debris flow	Low
6	Sandly silt	Slope of fault scarp	Eolian infall, later redeposited by slope-wash at foot of fault scarp (colluvium)	High
7	Pebbly sand	Slope of fault scarp	Mixture of creep, rainsplash, slopewash, and minor debris flow deposition (colluvium)	Moderate

* Numbers correlate with those on Figure 4.

† Inferred intensity and duration of sunlight exposure during deposition, based on our interpretation of depositional environment. Higher intensities associated with eolian or very shallow water deposition lead to greater degrees of initial "zeroing" of TL signal in those sediments.

subsequent to their last exposure to some bleaching mechanism, usually sunlight exposure. Aitken (1985) provides a comprehensive review of TL dating; Forman *et al.*, (1989) give additional information on the applicability of TL to neotectonic studies in the Basin and Range Province. All TL analyses were performed by Alpha Analytic, Inc., of Coral Gables, Florida. Laboratory methods are summarized in Appendix 2.

In evaluating the TL data from Alpha Analytic, we examined each of the 52 data plots of TL as a function of radiation dose that were used to calculate the equivalent dose (ED) values of Table 2. We noted that in most cases ED values calculated using the regeneration technique were inconsistent with, and lower than, ED values calculated using the other methods. Recent TL research indicates that the regeneration technique tends to underestimate true ages because of a possible instability in the TL signal (Debenham, 1985) or laboratory-induced sensitivity changes (Wintle, 1985; Rendell and Townsend, 1988). Therefore, we excluded these ED values from further analysis.

On the remaining 38 ED plots, we examined the statistics of the regression lines used to calculate the ED. If the coefficient of variation of the regression line was greater than 20 per cent, we felt that there was sufficient statistical uncertainty to render the ED calculation questionable. We found this condition on either the total or partial bleach ED plots of samples 3213, 3214, 3215, 3219 and 3220 (Table 2). In addition, most of these same plots exhibited a long extrapolation of the regression line from the natural to the residual TL level

TABLE 2

EQUIVALENT DOSE DATA FOR SEDIMENTS FROM THE EAST CACHE FAULT

Lab #	ED Method*	Bleach Procedure†	Temperature (°C)‡	ED (Grays)§	% Fading¶
3211	P. bleach	18hr/3-73	250-350	77.5 ± 47.7	< 5
	P. bleach(2)	45min/glass	250-350	74.0 ± 37.7	
	T. bleach	18hr UV	260-350	43.8 ± 32.2	
	Regen.	18hr UV	250-350	104.6 ± 23.9	
3212	P. bleach	18hr/3-73	250-300	22.0 ± 3.6	< 5
	T. bleach	18hr UV	240-300	32.2 ± 2.9	
	Regen.	18hr UV	240-310	34.6 ± 2.8	
3213	P. bleach	18hr/3-73	260-330	64.4 ± 44.2	< 5
	P. bleach(2)	45min/glass	270-350	35.2 ± 14.6	
	T. bleach	18hr UV	270-350	29.3 ± 10.7	
	Regen.	18hr UV	250-310	30.4 ± 6.0	
3214	P. bleach	18hr/3-73	280-330	71.2 ± 40.0	< 5
	T. bleach	18hr UV	250-350	68.8 ± 34.1	
	Regen.	18hr UV	280-360	95.1 ± 17.3	
3215	P. bleach	18hr/3-73	250-350	39.8 ± 26.4	10
	P. bleach(2)	45min/glass	290-370	18.2 ± 16.5	
	T. bleach	18hr UV	250-350	31.9 ± 14.5	
	Regen.	18hr UV	250-310	52.8 ± 6.0	
3216	P. bleach	18hr/3-73	260-320	19.1 ± 4.2	< 5
	P. bleach(2)	45min/glass	260-350	17.4 ± 6.8	
	T. bleach	18hr UV	250-320	22.5 ± 7.7	
	Regen.	18hr UV	250-310	26.4 ± 3.1	
3217	P. bleach	18hr/3-73	250-350	33.3 ± 6.1	
	P. bleach(2)	45min/glass	250-350	36.9 ± 7.0	10
	T. bleach	18hr UV	270-380	34.4 ± 5.1	
	Regen.	18hr UV	250-320	36.4 ± 3.1	
3218	P. bleach	18hr/3-73	250-350	10.8 ± 3.2	10
	P. bleach(2)	45min/glass	260-350	10.7 ± 3.0	
	T. bleach	18hr UV	250-320	11.6 ± 3.0	
	Regen.	18hr UV	250-350	13.6 ± 7.1	
3219	P. bleach(2)	45min/glass	270-390	39.8 ± 24.6	< 5
	T. bleach	18hr UV	250-300	45.5 ± 22.6	
	Regen.	18hr UV	250-390	62.6 ± 18.4	
3220	P. bleach(2)	18hr/3-73	270-390	27.3 ± 11.5	< 5
	T bleach	18hr UV	260-350	58.0 ± 8.3	
	Regen.	18hr UV	250-350	50.3 ± 5.4	
3221	P. bleach	18hr/3-73	250-320	44.6 ± 10.8	< 5
	P. bleach(2)	45min/glass	250-320	47.0 ± 21.4	
	T. bleach	18hr UV	250-320	57.5 ± 9.4	
	Regen.	18hr UV	250-320	58.4 ± 6.2	
3222	P. bleach	18hr/3-73	250-330	30.4 ± 13.5	10
	P. bleach(2)	45min/glass	280-350	41.7 ± 35.0	
	T. bleach	18hr UV	250-320	34.2 ± 7.2	
	Regen.	18hr UV	250-400	41.1 ± 2.7	
3209	P. bleach	18hr/3-73	240-310	89.6 ± 30.6	< 5
	P. bleach(2)	45min/glass	280-350	87.5 ± 21.1	
	T. bleach	18hr UV	250-320	82.4 ± 19.1	
	Regen.	18hr UV	250-350	59.0 ± 6.9	
3210	P. bleach	18hr/3-73	240-310	169.4 ± 32.4	< 5
	P. bleach(2)	45min/glass	250-350	170.9 ± 24.0	
	T. bleach	18hr UV	250-350	165.9 ± 24.0	
	Regen.	18hr UV	250-350	128.4 ± 7.6	

* Measurements were made with a Schott UG11 filter in front of the photomultiplier tube. All samples were preheated at 230° C for 1 min. P. bleach = Partial bleach, T. bleach = total bleach, Regen = regeneration.

† 18hr/3-73: 18 hour exposure to a 240 watt UV light source, 10 cm above the sediment with a Corning CS3-73 filter placed over the sediment. This filter has a cutoff at 420 nm (< 10% transmission for wavelengths below 425 nm). 45 min/glass: 45 minute exposure to a 240 watt UV light, 15 cm above the sediment with a 3/16″ glass plate over the sediment. 18hr UV: 18 hour exposure to 240 watt UV light source.

‡ Temperature region of the ED plot corresponding to the plateau region.

§ Mean and one sigma error for equivalent dose. Error is the mean of errors for ED determinations for temperature region.

¶ % anomalous fading with a > 21 day delay postirradiation.

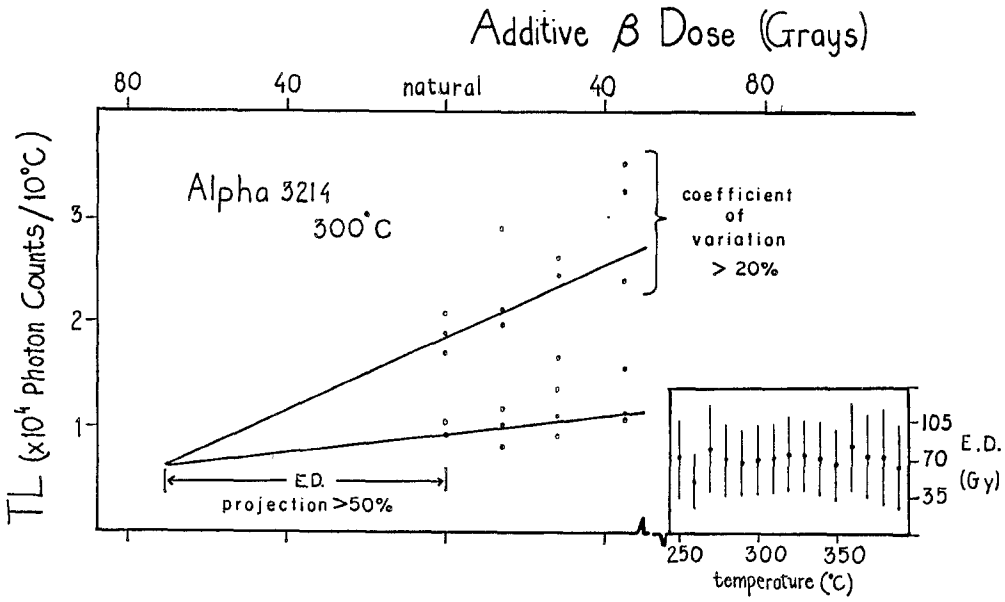

FIG. 5. Example of a typical unacceptable additive dose and partial bleach plot not used to calculate a TL age estimate. The equivalent dose (ED) projection is greater than 50 per cent of total regression line length and data points exhibit a coefficient of variation greater than 20 per cent. Inset plot is equivalent dose plotted at various temperatures.

(Fig. 5). Because we cannot always be certain that TL response is linear with radiation dose (even at these relatively low-dose levels), we judge ED plots, where the projected part of the linear regression line comprised more than 50 per cent of the total calculated regression, to be unreliable. Berger *et al.* (1987) suggest an even more conservative limit of 20 per cent, but with less stringent limits on coefficient of variation. Figure 5 shows a typical unacceptable ED plot exhibiting > 20 per cent coefficient of variation and > 50 per cent projection of the partial bleach regression line. Although these two statistical criteria are admittedly arbitrary, they represent a "first cut" for sorting out poorly constrained EDs. ED plots for the remaining eight samples generally exhibited better constrained statistics (< 20 per cent coefficient of variation, < 50 per cent projection to the residual level). An example of a reliable plot is given in Figure 6.

We then evaluated each sample for correspondence between the total bleach-based and two partial bleach-based ED values. If all three ED values are similar, the sediment was presumably well-bleached prior to deposition, and the initial "zeroing" requirement of the TL dating method is satisfied. This correspondence (at 1 sigma) occurs in seven of the eight samples exhibiting acceptable ED statistics. Because these samples are hillslope colluviums having a significant slopewash component (3209, 3210, 3218) or loess component (3216, 3217, 3222; see Fig. 4 and Table 1), their apparent high initial bleaching is not surprising. Only sample 3212 from unit 4 exhibits a significantly larger total bleach ED value than partial bleach value. This discordance usually indicates that the laboratory total bleach (which simulates intense direct sunlight exposure) is much stronger than the sunlight exposure actually received by the sediment prior to deposition (i.e., laboratory overbleaching). Based on

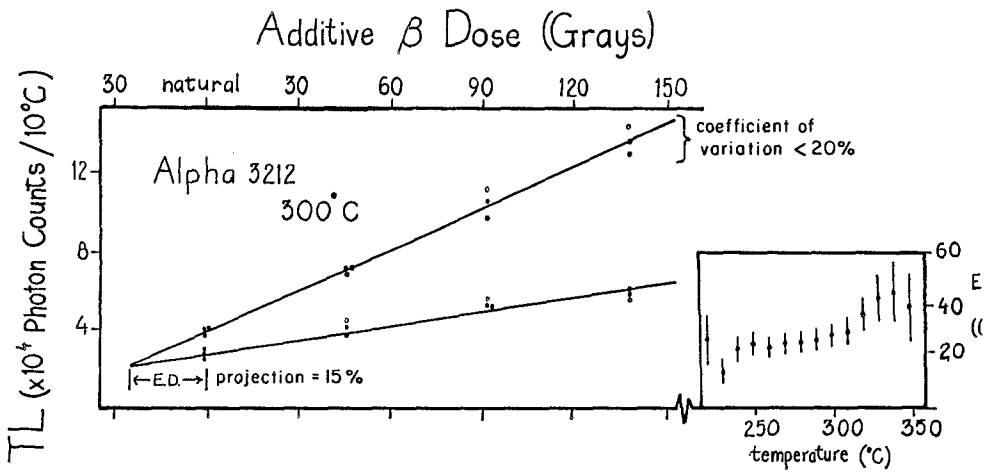

FIG. 6. Example of a typical acceptable additive dose and partial bleach plot used to calculate equivalent dose and resultant TL age estimates (Table 4). The equivalent dose (ED) projection is less than 20 per cent of the maximum additive dose and data points exhibit a coefficient of variation of less than 20 per cent. Inset plot is equivalent dose plotted at various temperatures.

our interpretation of the sedimentology of unit 4, we infer that disruption and remobilization of the sand on the margins of the tectonic "melange," where sample 3212 was collected, was insufficient to re-expose all silt grains to solar radiation (see following section).

Because all of the eight samples having acceptable ED statistics received some degree of (but not complete) predepositional bleaching, our preferred ED estimate is that calculated by the short subaerial exposure partial bleach method (18 hr/3-73 of Table 2). Previous studies (Berger *et al.*, 1984; Forman *et al.*, 1987) demonstrated that the partial bleach procedure is most conservative for not overbleaching in the laboratory and yields apparently accurate results.

The last step before calculating a TL age estimate is evaluating for anomalous fading, which is a short-term instability in the laboratory-induced TL signal (Wintle, 1973). Alpha Analytic checked for anomalous fading after storing irradiated samples for the standard 21-day period (Lamothe, 1984). While most samples exhibited negligible fading (< 5 per cent), samples 3217, 3218, and 3222 exhibited approximately 10 per cent fading.

TL age estimates (Table 4) for the eight samples exhibiting acceptable ED statistics were calculated by dividing the partial bleach ED (18 hr/3-73 in Table 2) by the contemporary dose rate (DR) modified for postdepositional water content (Table 3). For those samples exhibiting 10 per cent fading, the age estimates in Table 4 may be underestimates of the true age by approximately 10 per cent.

CHRONOLOGY OF FAULTING

Two faulting events are recognized in the Logan trench. We hereby summarize evidence that constrains the timing of each event, based on: (1) stratigraphic relations in the Logan trench, (2) one radiocarbon age and eight TL age estimates from the Logan trench, and (3) geomorphic relations between fault scarps and Quaternary deposits in the central section.

TABLE 3

DOSE RATE DATA FOR SEDIMENT SAMPLES FROM EAST CACHE FAULT ZONE

Lab #	Bulk alpha count rate (ks cm^{-2})	Th* (ppm)	U* (ppm)	U/S†	%K_2O	% H_2O‡	a value§	DR¶ Gy/ka
3209	0.74 ± 0.01	5.5 ± 1.1	4.6 ± 0.3	0.96	1.95 ± 0.02	20 ± 5	0.05 ± 0.01	3.48
3210	0.71 ± 0.01	8.4 ± 1.3	3.5 ± 0.4	0.99	1.39 ± 0.02	20 ± 5	0.11 ± 0.01	3.72
3211	0.29 ± 0.01	2.1 ± 0.6	1.9 ± 0.2	0.95	0.72 ± 0.02	20 ± 5	0.08 ± 0.02	1.59
3212	0.39 ± 0.01	4.3 ± 0.8	2.0 ± 0.2	0.98	0.72 ± 0.02	15 ± 5	0.07 ± 0.01	1.89
3213	0.32 ± 0.01	1.9 ± 0.6	2.1 ± 0.2	0.93	0.82 ± 0.02	20 ± 5	0.08 ± 0.02	1.73
3214	0.40 ± 0.01	5.8 ± 1.1	1.6 ± 0.3	1.00	0.95 ± 0.02	20 ± 5	0.05 ± 0.01	1.86
3215	0.40 ± 0.01	1.1 ± 0.5	3.0 ± 0.2	0.85	0.80 ± 0.02	20 ± 5	0.08 ± 0.01	1.90
3216	0.48 ± 0.01	5.4 ± 1.0	2.5 ± 0.3	0.98	0.78 ± 0.02	15 ± 5	0.12 ± 0.01	2.66
3217	0.62 ± 0.01	7.9 ± 1.1	2.9 ± 0.3	0.96	1.47 ± 0.02	20 ± 5	0.10 ± 0.01	3.33
3218	0.71 ± 0.01	8.0 ± 1.1	3.6 ± 0.3	1.06	1.82 ± 0.02	20 ± 5	0.13 ± 0.01	4.27
3219	0.84 ± 0.02	5.0 ± 1.0	2.3 ± 0.3	0.99	0.84 ± 0.02	20 ± 5	0.12 ± 0.01	2.43
3220	0.49 ± 0.01	5.4 ± 1.0	2.5 ± 0.3	0.97	0.97 ± 0.02	20 ± 5	0.14 ± 0.01	2.94
3221	0.48 ± 0.01	6.7 ± 1.1	2.0 ± 0.4	0.96	0.80 ± 0.02	15 ± 5	0.11 ± 0.01	2.56
3222	0.48 ± 0.01	6.1 ± 1.1	2.2 ± 0.3	1.04	0.93 ± 0.02	20 ± 5	0.26 ± 0.07	3.76

* Th and U calculated from bulk alpha count rate, assuming secular equilibrium.

† Unsealed versus sealed alpha count ratio, ratio < 0.95 indicates significant radon loss.

‡ Long-term water content (weight of water/weight of dry sediment). Estimated as 15 ± 5% for freely-draining sands with 1 m of ground surface (above moisture line in trench); 20 ± 5% for all other samples.

§ The measured alpha efficiency factor as defined by Aitken and Bowman (1975).

¶ Dose rate which includes contribution from cosmic rays of 0.14 ± 0.01 Gy/ka. All errors are one sigma.

TABLE 4

EQUIVALENT DOSE (ED) BY THE PARTIAL BLEACH METHOD (18HR/3-73) AND TL AGE ESTIMATES FOR SEDIMENTS FROM THE EAST CACHE FAULT ZONE

Lab #	ED (Grays)	TL Age estimates (ka)
3209	89.6 ± 30.6	25.8 ± 7.6
3210	169.4 ± 32.4	45.6 ± 7.0
3212	22.0 ± 3.6	11.6 ± 1.7
3216	19.1 ± 4.2	7.5 ± 1.3
3217	33.3 ± 6.1	10.0 ± 1.6*
3218	10.8 ± 3.2	2.5 ± 0.5*
3221	44.6 ± 10.8	17.4 ± 3.0
3222	30.4 ± 6.7	8.1 ± 1.6*

* Samples exhibiting 10% anomalous fading. Ages quoted are probably underestimates by roughly 10%.

Age estimates are only calculated for samples which display statistically acceptable ED calculations (as defined in the text). All errors are one sigma, following the method of Aitken (1985, pp. 241-250).

Earlier Faulting Event on the Central Section

The log of the Logan trench (Fig. 4) shows that the lacustrine sands (units 1 and 2) have been faulted about 4.3 m down to the west. We infer that, prior to faulting, the trench site was occupied by a north-trending littoral bar, cored with horizontally bedded sand (units 1 and 2) and veneered with a "shell" of

gravel with opposing cross-bed directions (units 3a, 3b). The earlier faulting event produced a cumulative stratigraphic displacement of 3.14 m on faults D, E, and F (Fig. 4c) and displaced the bar near its center, exposing the sand core in the free face. The exposed sand core presumably failed rapidly in an avalanche of loose sand and sand blocks to form unit 4 and its basal unconformity. This highly-mixed "melange" of sand and sand blocks, plus the presence of sand-blow-like features, suggested to us initially that faulting had occurred under water. Geomorphic relations (described later) show that lake level had abandoned this surface by the time of faulting, so liquefaction features may have resulted from local groundwater saturation. Unit 5, present only on the downthrown block, was probably derived from the gravel that covered the bar crest, which after faulting slid downslope as a thin debris flow (Fig. 4b). Following deposition of units 4 and 5, the scarp profile declined due to subaerial erosion, and unit 6 (the silty colluvium) was deposited against and across the scarp. Thus the earlier faulting event postdates units 1, 2, and 3, is contemporaneous with unit 4 (and possibly 5), and predates unit 6.

Two TL age estimates on unit 4 that should be contemporaneous with faulting are somewhat contradictory. Sample 3221 from the lateral equivalent of the sand blow from fault B (Fig. 4c) yielded a TL age estimate of 17.4 ± 3.0 ka (Table 4). This date is older than that of stratigraphically lower unit 3b and appears to be erroneously old. The geometry shown in Figure 4c suggests that the blow sand was ejected onto the surface of the sandy "melange" (unit 4) from a source bed within unit 1, probably near the base of the fault B sand-blow chimney (Fig. 4c). Eyewitness accounts of sand extrusion in historic earthquakes (e.g., Fuller, 1912) suggest that during sand blow deposition a majority of sand grains probably would not receive sufficient (> 8 hours) new sunlight exposure to "re-zero" the TL signal. As a result, the TL age estimate for sample 3221 may more closely date the initial deposition of the lacustrine sand (in a stratigraphically low position somewhere within unit 1) than its redeposition during faulting. Sample 3212 was collected from a thin distal part of the "melange" that exhibited weakly contorted but finely laminated medium to fine sand, which was quite distinct from the massive sand associated with the sand blows (Fig. 4c). The TL age estimate of 11.6 ± 1.7 ka (3212, Table 4) is reasonable compared to the age of underlying unit 3b (15,540 ± 130 yr BP; AA-4017) and overlying unit 6 (7.5 ± 1.2 ka, 3216 to 10.0 ± 1.5 ka, 3217; Table 4). Finally, three TL age estimates on the post-earlier event colluvium (unit 6) provide minimum ages on faulting. Samples 3216 and 3222 from near the base of unit 6 on the downthrown and upthrown blocks, respectively, yield similar estimates of 7.5 ± 1.2 ka (3216) and 8.1 ± 1.6 ka (3222) (Fig. 4c); however sample 3222 exhibited > 10 per cent fading and may be somewhat older (Table 4). The 10.0 ± 1.5 ka age estimate for sample 3217 comprises a weak apparent chronologic reversal (not significant at 1 sigma). That sample represents a chunk of soil horizon, which we infer fell from the second-event free face, hence its original stratigraphic position is unknown. In light of the age spread of these dates, we assign the mean (including a 10 per cent increase for fading in samples 3217 and 3222) of 8.7 ± 1.0 ka as the age of the basal part of unit 6.

Stratigraphic and numerical-age data from the Logan trench thus bracket the earlier faulting event between a mean TL age estimate of 8.7 ± 1.0 ka (3216, 3217, and 3222) and a radiocarbon age of 15,540 ± 130 by BP (AA-4017), with the suggestion that a deposit dated at 11.6 ± 1.7 ka (3212) is contemporaneous

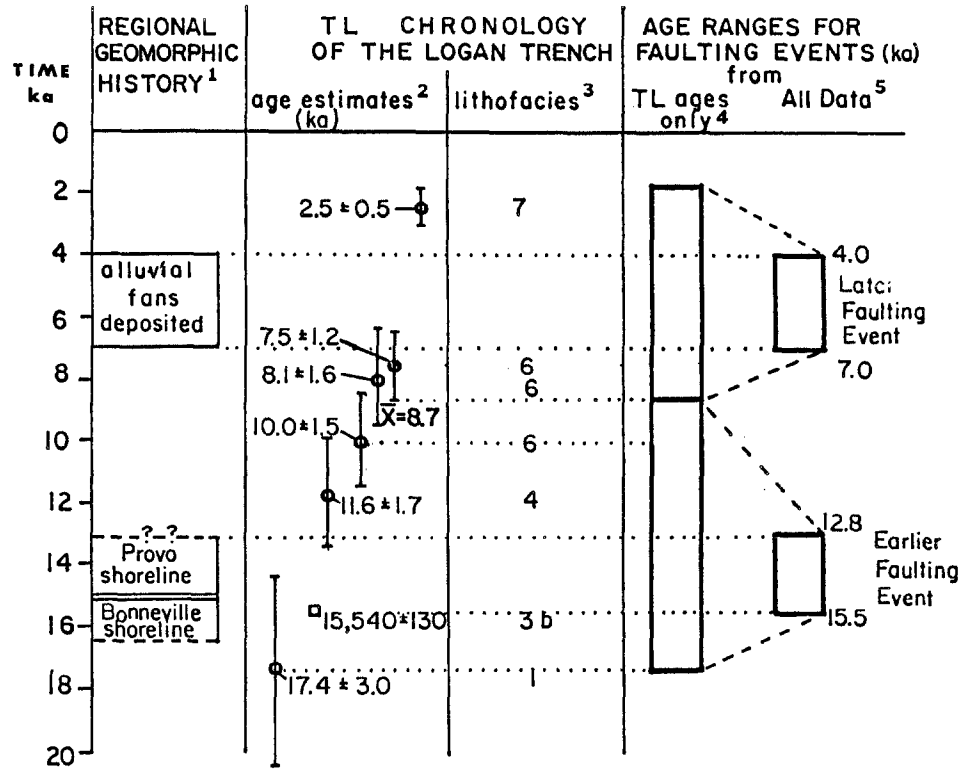

FIG. 7. Diagram of bracketing ages for the two surface faulting events exposed in the Logan trench. [1]Regional geomorphic history based on radiocarbon dates from Currey and Oviatt (1985), Machette *et al.* (1987), and Currey and Burr (1988). The end of Provo shoreline occupation (marked with question marks) is defined by the oldest date on post-Provo regressive deposits (12.8 ka) as shown in Figure 1 of Currey and Oviatt (1985). [2]TL age estimates from Table 4; length of bar is ± one sigma; open square is an accelerator mass spectrometry radiocarbon age on gastropod shells. [3]Units dated by the TL age estimate (at left) from Logan trench; see Figure 4. [4]Age ranges bracketed by the youngest probable age (± one sigma) of the oldest unfaulted deposit and the oldest probable age of the youngest faulted deposit, as measured by TL. [5]Age range incorporating additional age constraints from cross-cutting relationships between fault scarps, and alluvial fans and deltas dated by correlation to the regional Lake Bonneville chronology.

with faulting (Fig. 7). An additional age constraint is imposed by the observation of Swan *et al.* (1983) that fault scarp heights are twice as large on the Bonneville highstand delta than on the Provo-level delta (Fig. 3). This geometry implies that the earlier faulting event expressed on the Bonneville highstand delta at the trench site predated the formation of the Provo delta surface. Currey and Oviatt (1985) bracket the occupation of the Provo delta shoreline between about 12.8 and 13.4 ka. The additional geomorphic constraint suggests the earlier faulting event on the central section occurred between about 12.8 to 13.4 ka and 15,540 ± 130 yr BP (AA-4017). The TL age estimate from the syntectonic (?) unit 4 (sample 3212, 11.6 ± 1.7 ka) overlaps the youngest part of this age range at one sigma (Fig. 7) showing that, in the absence of other supporting data, the TL age estimate is marginally useful (at 1 sigma) in dating this faulting event.

Later Faulting Event on the Central Section

In the Logan trench, the early loess-rich colluvium (unit 6) has subsequently been displaced along faults E and F and the unconformity at the base of unit 4

TABLE 5

VERTICAL DISPLACEMENTS ON INDIVIDUAL FAULTS AND ACROSS ENTIRE DEFORMATION ZONE, LOGAN TRENCH

	Vertical Displacement (cm)		
	Total	In Earlier Event	In Later Event
Synthetic Faults			
A	26	0	26
B	9	0	9
C	2	0	2
D	105	105	0
E	28	4	24
F	260	205?	55?*
Synthetic total =	430	314	116
Antithetic Fault	−80	−40?†	−40?
Backtilting‡	−95	−95	0
Net across Entire Zone =	255	179	76

* Questionable value, measured as vertical difference between the base of unit 6 on either side of the tension crack fill between faults E and F. If the base of unit 6 had an original valleyward gradient (probable), then 55 cm is a maximum value.

† Estimated value, assuming half of total displacement occurred in each event. The ground surface and unit 5 are weakly warped over the fault, suggestive of minor displacement during the second event.

‡ Backtilting of the downthrown block of roughly 4° (based on divergence of unit 5/3b contact from the ambient faulted surface) over a horizontal distance of 13.5 m (see Fig. 4) results in 95 cm of tilt-induced slip on fault F. Because the top of unit 6 has a similar gradient to that of the modern ground surface, it is assumed to be untilted, and thus all tilt is assigned to the earlier faulting event.

displaced by faults A, B, and C (Fig. 4c). The sand blow-like features emanating from faults A and B are associated with 35 cm vertical displacement. In the fault B sand blow, a discrete fault plane can be traced upwards through the sand blow material (Fig. 4c) and the overlying upper contact of unit 6 is warped, indicating that the 9 cm of vertical displacement on fault B occurred during the later faulting event. By noting differential vertical displacements between marker beds in unit 1 and the unconformity at the base of unit 4, displacements can be partitioned between the earlier and later faulting events (Table 5).

Prior to the later faulting event a strong soil profile had developed on unit 6. This soil (horizons B1k, B2k, K; Fig. 4c) is now only preserved on the downthrown block; presumably the soil on the upthrown block was eroded following the second faulting event. A displaced piece of Bk horizon (between TL samples 3217 and 3218, Fig. 4c) appears to be a chunk of the upthrown-block soil that fell to the base of the free face following the later faulting event. No discrete wedge of colluvium was deposited after the later faulting event. Instead, it appears that much of the earliest-derived colluvium from the free face fell into a tension gap between faults E and F (Fig. 4c). Later colluvium is spread as a relatively uniform layer over the entire scarp face (unit 7). This lack of a wedge-shaped colluvial deposit is often associated with multiple small-displacement faulting (≤ 1.0 m) on a pre-existing slope (Ostenaa, 1984; McCalpin, 1987b). The youngest slope colluvium (unit 7) bears a moderately developed soil with a cambic B horizon, suggestive of several thousand years of weathering (Shroba, 1980).

The mean of TL age estimates for the basal part of unit 6 (8.7 ± 1.0 ka) provides a maximum limiting age for the later faulting event. The lower part of unfaulted unit 7 yields a TL age estimate of 2.5 ± 0.5 ka (3218). This sample postdates faulting by the time needed to degrade the free face created by faults E and F and to deposit the lower half of unit 7. The time window 2.5 to 8.7 ka is too large to tightly constrain faulting, so we again turn to geomorphic evidence to decrease the time interval.

Holocene alluvial fans along the ECFZ are not faulted; their age (if known) would provide another minimum limiting date on faulting. Two generations of Holocene fans were mapped by McCalpin (1989), an early-middle Holocene set (af_1) and late Holocene set (af_2; Fig. 3). These fans are undated, but preliminary evidence from the nearby Wasatch fault zone suggests that many early-middle Holocene fans were deposited between ca. 4 and 7 ka (Machette *et al.*, 1987; Nelson, 1988; Personius, 1988). If ECFZ fans are of similar age, then the later faulting event may be older than ca. 4 ka. Such a minimum age is reasonably consistent with the degree of soil development on postfaulting colluvium (unit 7) and with the minimum TL age estimate of 2.5 ± 0.5 ka (3218). Figure 7 summarizes the limiting dates for the two latest faulting events on the central section based on all available data.

Quaternary Faulting on the Northern and Southern Sections

No late Quaternary surfaces are displaced in the northern and southern sections of the ECFZ, but several artificial exposures show that underlying Quaternary sediments are faulted. A gravel pit near High Creek in the northern section (location 1, Fig. 2) reveals a complex graben zone 30-m wide in a Provo-level delta deposit (Fig. 8). All faults are truncated by channels near the delta surface; these channels are restricted to the topographic depression formed by the graben. The faults have no surface expression north or south of the gravel pit, despite the fact that the gently sloping Provo delta surface is well

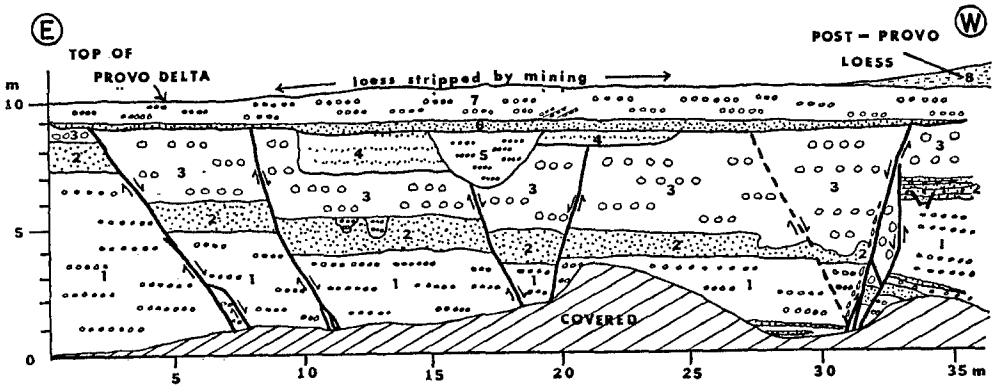

FIG. 8. Sketch of fault relations on the south wall of the Zan Christensen gravel pit, north side of the mouth of High Creek (exposure 1 on Figure 2). Large open circles indicate coarse pebble gravel, smaller circles indicate small pebble gravel, and stipples indicate medium to fine sand. Numbered units 1 through 3 are laterally extensive. To the right (west) of the exposure, they grade into west-dipping foreset beds of the delta front. Units 4 through 6 are channel fills confined to the graben. Unit 7 is topset beds of the Provo delta and is overlain (where not removed by humans) by up to 1 m of post-Provo loess. Faults displace only units 1 to 3 and clearly predate the latest deltaic topset beds.

preserved over a distance of 2 km (McCalpin, 1989). These relationships suggest that the faults formed late during the deposition of the Provo delta, while the delta surface was still active. After faulting, the active delta channels were diverted into the graben where they deposited several channel fills. Late Provo topset beds subsequently covered the entire deposit. No numerical ages were obtained from this short-lived exposure. Based on Currey and Oviatt's (1985) dates on Provo deposits as 12.8 to 13.4 ka, the age of late Provo faulting here can be estimated as ca. 13 ka.

This gravel pit exposure (and a similar one 1-km south) raises several questions. (1) If surface-faulting occurred on the northern section ca. 13 ka, why are no fault scarps observed in Bonneville highstand deposits along the range front (McCalpin, 1989)? (2) Why is faulting found only near the front of Provo level deltas roughly 1 km valleyward of the range-front escarpment? (3) Is the similarity of inferred fault timing on the northern section (ca. 13 ka) and on the central section (12.8 ka to 15.5 ka) coincidental? All three questions can be answered satisfactorily if the graben faults represent merely lateral spreading of the delta front during seismic shaking and not surface-rupture on the northern section. Seismic shaking from the earlier faulting event on the central section could easily have produced lateral spreading in an active Lake Bonneville delta, which lies only 20-km north of the central section.

Several artificial exposures on the southern section of the ECFZ expose faults, but none of them clearly indicates late Quaternary surface rupture. The 11-m-high cuts for water tanks 2 km east of Hyrum (immediately south of the central/southern section boundary) expose multiple faults that displace Bonneville shoreline deposits a total of 1.6 m down to the west. These faults all dip 35° west (unusually shallow for normal faults in unconsolidated deposits; McCalpin, 1987c) and do not displace the ground surface. They may be lateral spread or slump features similar to those observed in the northern section, or they may represent surface rupture from the central section that extended barely across the boundary into the southern section.

Canal bank cuts in the center of the southern section at East Fork (location 2 on Fig. 2) also expose multiple faults along the active trace. The active trace north and south of the cuts is marked by saddles and subdued fault scarps in presumed middle Pleistocene pediment surfaces, but no scarps exist across deposits of the Bonneville lake cycle or of Holocene age (McCalpin, 1989). Cuts expose a lower, pervasively sheared colluvium unconformably overlain by a similar, but unfaulted, hillslope colluvium. TL data on samples from the lower and upper colluviums at location 2 on Fig. 2 (3210 and 3209, respectively; Tables 2, 3, and 4) display statistically well-constrained ED plots and show a good correspondence between total bleach and partial bleach EDs, indicating that the deposits were well bleached prior to deposition. TL age estimates of 25.8 ± 7.5 (3209) and 45.6 ± 7.0 (3210) ka bracket the latest displacement on these faults.

This age of latest faulting is compatible with the lack of fault scarps across deposits of the Bonneville lake cycle (13 to 30 ka) on the southern section. The age range is also roughly compatible with the age of latest faulting on the James Peak fault, estimated by Nelson and Sullivan (1987) at between 30 and 70 ka (but nearer the younger age). Despite the poor age control, it appears that neither of the two paleoseismic events identified on the central section (ca. 4 to ca. 7 ka; ca. 13 ka to 15,540 ± 130 yr BP) produced observable rupture on the

TABLE 6

INFERRED MAGNITUDES OF PALEOEARTHQUAKES ON THE CENTRAL SEGMENT OF THE ECFZ

	Displacement per Event		Estimated Seismic Moment*	Inferred Moment Magnitude†	Inferred Magnitude		
	Vertical (m)	Net Slip§ (m)	M_0 (dyne-cm)	M_w	M_s‡ (from Bonilla *et al.* 1984)	M_s‡ (from Slemmons, 1982)	M_L (from Khromovskikh, 1989)
Earlier Event at Trench	1.8	1.9	1.88×10^{26}	6.8	7.0¶	6.9#	
Later Event at Trench	0.8	0.9	1.04×10^{26}	6.6	6.8¶	6.7#	
Later Event on Provo delta	1.4	1.6	1.69×10^{26}	6.8	7.0¶	6.8#	
Probable Maximum Paleoevent	2.1[c]	2.4	2.53×10^{26}	6.9	7.1¶	6.9#	
Minimum length of rupture (km)			8		6.7[a]	6.0[b]	6.6[d]
Probable length of rupture (km)			20		7.0[a]	6.6[b]	7.1[d]

* $M_0 = M * A * D$, where M = elastic modulus = 3×10^{11} dyne/cm^2 (Arabasz *et al.*, 1979); A = area of fault plane, assuming length of 20 km, depth of 15 km, dip of 60°; D = displacement (net slip).

† $M_w = 2/3$; $M_0 - 10.7$ (Hanks and Kanamori, 1979).

‡ Inferred from regression of M_s on log of displacement from historic earthquakes.

§ Assuming 60° dip of causative fault at seismogenic depths.

¶ Normal fault data only, ordinary least squares regression; $M_s = 6.71 + 0.741 \log d$ (m).

Normal fault data only; $M_s = 6.668 + 0.75 \log d$ (m).

[a] Plate interior faults only, ordinary least squares regression; $M_s + 6.02 + 0.729 \log L$ (km).

[b] Normal fault data only; $M_s = 0.809 + 1.341 \log L$ (m).

[c] Probable maximum per-event displacement in late Quaternary time, estimated by partitioning the maximum observed vertical surface displacement (4.2 m) equally between two events.

[d] Faults of "ancient platforms rejuvenated in Cenozoic"; $M_L = 5.45 + 1.25 \log L$ (km).

southern section. It is possible that the latest rupture on the James Peak fault also ruptured the southern section, suggesting a maximum total rupture length of about 34 km.

Paleoearthquake Magnitude and Recurrence

Paleoearthquake magnitude on the ECFZ can be inferred from estimates of the maximum displacement per event or the length of surface rupture (world-wide data set of Bonilla *et al.*, 1984). The earlier paleoearthquake on the central section, based on a minimum of 1.79 m displacement at the Logan trench and a rupture length of at least 8 km (20 km if entire section ruptured), yields M_s 6.8 and M_s 6.0 to 7.1, respectively (Table 6). The later event on the central section (maximum observed vertical displacement 1.4 m, unknown lateral extent) yields a similar value of M_s 6.8 to 7.0. Field relations indicate that both of these ruptures were limited to the 20-km-long central section; a 20-km length of surface rupture corresponds to earthquakes of M_s 6.6 to 7.1 (Table 6) and displacement of roughly 1.0 to 1.5 m. Thus the displacements inferred for individual paleoseismic events on the central section are compatible with segment length and suggest events in the range of M_s 6.6 to 7.1.

The three section subdivision of the ECFZ proposed in the Introduction is defined by changes in fault zone complexity (change from a single trace to multiple traces) and by the absence of late Pleistocene fault scarps in the northern and southern sections. However, the structure of range front faceted spurs is quite similar for the central and southern sections. Gravity data (Mabey, 1985) show that no subsurface gravity saddle exists between the central and southern sections, although on the Wasatch fault zone such saddles typically mark boundaries between seismogenic segments (Wheeler and Krystinik, 1988). These observations suggest that through much of late Cenozoic time the central and southern sections, which have a combined length of 44 km (51 km if the James Peak fault is included), may have acted as a single seismogenic segment. Late Pleistocene fault scarps on the central section do *not* extend into the southern section. Rupture terminations indicate that in the last two ruptures the central section has acted as a seismogenic segment, but over the entire Quaternary the central/southern section boundary has been nonpersistent. In contrast, the boundary between the central and northern sections is marked by a gravity saddle in Cache Valley (Mabey, 1985) and by a significant decrease in the complexity of and number of range-front faceted spurs. This boundary may be a persistent segment boundary between the 20-km-long central segment and the northern section composed of one or more seismogenic segments.

The hypothetical multi-segment ruptures, such as a 25 ka to 45 ka(?) event involving the James Peak fault and southern section of the ECFZ (length 34 km) or a combined central/southern section rupture (length 44 km) imply larger earthquakes. Nelson and Sullivan (1987) noted that the discrete displacements of 1.8 and 2.4 m inferred on the James Peak fault were anomalously large for the 7- to 10-km length of the fault, and they hypothesized that such events also ruptured the southern section of the ECFZ. Displacements of 1.8 to 2.4 m are associated with surface rupture lengths of 39 to 45 km (Bonilla *et al.*, 1984), lengths which are more similar to the combined James Peak fault/southern section length of 34 km than to the individual lengths of either section (10 km, 24 km). These larger earthquake events (M_s 7.2) may have recurrence intervals of 50 ka or more (Nelson and Sullivan, 1987).

The two dated paleoearthquakes on the central segment (ca. 4 to ca. 7 ka; ca. 13 ka to 15,540 ± 130 yr BP) define only a single dated recurrence interval between events (minimum 5.8 ka, maximum 11.5 ka). The elapsed time since the most recent event (ca. 4 to ca. 7 ka) constitutes as little as 34 per cent to as much as 120 per cent of the maximum and minimum recurrence estimates, respectively. Given the uncertainties in dating the latest two paleoearthquakes, we cannot presently state whether the ECFZ is in the beginning, middle, or near the end of a stress-release cycle.

Implications for Faulting within the Northern Wasatch to Teton Corridor (NWTC)

Compared to other NWTC faults, the ECFZ exhibits anomalously small slip values during the past 15 ka. The maximum surface offset on fault scarps of the central segment (4.2 m) on Bonneville highstand deposits (15.5 ka) equates to a slip rate of 0.27 m/ka. In contrast, the nearest segment of the Wasatch fault (Brigham City segment) exhibits scarps up to 22-m high across Provo-level deltas (13 ka), yielding a slip rate of roughly 1.7 m/ka (Personius, 1988).

Ongoing work by McCalpin *et al.* (1990a) on the eastern Bear Lake fault has documented about 10 m of normal fault displacement since 12.3 ka, for a slip rate of about 0.8 m/ka. Quaternary fault scarps up to 11-m high on the Star Valley fault across 10 to 15 ka deposits (Piety *et al.*, 1986) imply slip rates of 0.6 to 1.2 m/ka. The Teton fault, with displacements of up to 34 m in postglacial deposits has an estimated maximum slip rate of 1.7 to 2.2 m/ka (Gilbert *et al.*, 1986). Thus, in the last 15 ka, the slip rate on the central segment of the ECFZ has averaged only 16 per cent to 45 per cent of the slip rate on other NWTC faults.

Despite the small slip values on the ECFZ during the past 15 ka, the structural and topographic relief across the fault zone is similar to that of other NWTC faults. Total late Cenozoic slip on the ECFZ has been estimated at 3.4 to 4.5 km (Zoback, 1983; Evans, personal comm.) based on gravity and seismic reflection data. By comparison, late Cenozoic displacement on the Brigham City segment of the Wasatch fault, eastern Bear Lake fault, and Star Valley fault are estimated at 3.4 km (Zoback, 1983), 4.9 km (J. P. Evans, personal comm.) and 3.3 km (Piety *et al.*, 1986). If late Cenozoic slip rates are typical of the long-term behavior of NWTC fault blocks, then in the last 15 ka the ECFZ may have accumulated a considerable slip deficit in relation to its neighboring faults.

Conclusions

A trench across the central segment of the ECFZ revealed evidence of two paleoearthquakes during the past 15 ka. Thermoluminescence age estimates augmented by regional radiocarbon chronology suggest that the earlier event (net displacement 1.8 m at the trench) occurred between ca. 13 and 15.5 ka. The later event (net displacement 0.8 to 1.4 m) occurred between ca. 4 and ca. 7 ka. Age control for faulting events was available in two forms: (1) one radiocarbon and six TL age estimates from the trench and (2) correlation to radiocarbon-dated deposits elsewhere in the Bonneville Basin. The on-site TL age estimates were compatible with the on-site radiocarbon age and with the correlated regional radiocarbon chronology, but TL only defined broad age ranges during which faulting could have occurred. In contrast, geomorphic relations suggested tighter age bracketing of faulting events, but relied on an unproven correlation to radiocarbon-dated sites elsewhere. The general correspondence of both types of dating control strengthens our confidence in the final age assessments. TL dating thus provided an auxiliary role in this study, but would have been much more critical in an area without the well-dated radiocarbon chronology of the Bonneville Basin.

The calculated post-15-ka slip rate of the ECFZ appears anomalously low (0.27 m/ka) when compared to the late Cenozoic and post-15-ka slip rates of adjacent NWTC faults. The obvious way for the ECFZ to "catch up" with adjacent faults is to undergo significant fault slip in the future. However, the present poor dating control on the latest two paleoearthquakes precludes a precise estimate of our present chronologic position within a typical stress-release cycle.

Acknowledgments

We thank Jerry Stipp of Alpha Analytic, Inc., for providing all the raw laboratory data from the TL analyses. Margaret Berry and Mike Jackson (University of Colorado) and John Garr and John Rice (Utah State University) assisted in logging the Logan trench. Trenching and data analysis

were funded by USGS contracts No. 14-08-0001-G1096 and 14-08-0001-G1396, respectively. The manuscript benefited from critical reviews by S. N. Wesnousky, F. H. Swan III, and four anonymous reviewers.

References

Aitken, M. J. (1985). *Thermoluminescence Dating*, Academic Press, New York, 359 pp.

Aitken, M. J. and S. G. E. Bowman (1975). Thermoluminescence dating; assessment of alpha particle contribution, *Archaeometry* **17**, 132–38.

Arabasz, W. J., W. D. Richins, and C. J. Langer (1979). The Idaho-Utah border (Pocatello Valley) earthquake sequence of March-April, 1975, in *Earthquake Studies in Utah, 1850 to 1879*, W. J. Arabasz *et al.* (Editors), Special Publication, University of Utah Seismograph Station, Salt Lake City, Utah, 339–374.

Bailey, R. W. (1927). The Bear River Range fault, Utah, *Am. Jour. Sci.* **13**, 497–502.

Berger, G. W., D. J. Huntley, and J. J. Stipp (1984). Thermoluminescence studies on a 14-C-dated marine core, *Can. J. Earth Sci.* **21**, 1145–1150.

Bonilla, M. G., R. K. Mark, and J. J. Lienkaemper (1984). Statistical relations among earthquake magnitude, surface rupture length, and surface fault displacement, *Bull. Seism. Soc. Am.* **74**, 2379–2411.

Byrd, J. O. D. and R. B. Smith (1990). Dating recent faulting and estimates of slip rates for the southern segment of the Teton Fault, Wyoming, *Geol. Soc. Am. Abstr. Prog.* **22**, No. 6, 4–5.

Cluff, L. S., C. E. Glass, and G. E. Brogan (1974). Investigation and evaluation of the Wasatch fault north of Brigham City, and Cache Valley faults, Utah and Idaho, Woodward-Lundgren and Associates, report to the Utah Geological and Mineral Survey, Salt Lake City, Utah, 147 pp.

Currey, D. R. and T. N. Burr (1988). Linear model of threshold-controlled shorelines of Lake Bonneville, *Utah Geological and Mineral Survey, Misc. Publ.* **88-1**, 104–110.

Currey, D. R. and G. C. Oviatt (1985). Durations, average rates, and probable causes of Lake Bonneville expansions, stillstands, and contractions during the last deep-lake cycle, 32,000 to 10,000 years ago, in *Problems of and Prospects for Predicting Great Salt Lake Levels*, P. A. Kay and H. F. Diaz (Editors), Center for Public Affairs and Administration, University of Utah, Salt Lake City, Utah, May 1985, 9–24.

Debenham, N. E. (1985). Use of UV emissions in TL dating of sediments, *Nuclear Tracks and Radiation Measurements* **10**, 717–724.

Evans, J. P. and R. Q. Oaks (1990). Geometry of Tertiary extension in the northeastern Basin and Range Province superimposed on the Sevier Fold and Thrust Belt, Utah, Idaho and Wyoming, *Geol. Soc. Am. Abstr. Prog.* **22**, No. 6, 10.

Forman, S. L. (1989). Application and limitation of thermoluminescence to date Quaternary sediments, *Quaternary International* **1**, 47–59.

Forman, S. L., M. N. Machette, M. E. Jackson, and P. Maat (1989). An evaluation of thermoluminescence dating of paleoearthquakes on the American Fork segment, Wasatch fault zone, Utah, *J. Geophys. Res.* **94**, B2, 1622–1630.

Forman, S. L., A. G. Wintle, H. L. Thorleifson, and P. H. Wyatt (1987). Thermoluminescence properties and age estimates of Quaternary marine sediments from the Hudson Bay lowland, Canada. *Can. J. Earth Sci.* **24**, 2405–2411.

Fuller, M. L. (1912). The New Madrid earthquake, *U.S. Geol. Surv. Bull. 494*, 112 p.

Gilbert, J. D., D. A. Ostenaa, and C. K. Wood (1983). Seismotectonic study, Jackson Lake Dam and Reservoir, Minidoka Project, Idaho-Wyoming, *U.S. Bureau of Reclamation Seismotectonic Report 83-8,* 122 pp. and Appendices.

Hanks, T. C. and H. Kanamori (1979). A moment magnitude scale, *J. Geophys. Res.* **84**, 2981–2987.

Huntley, D. J. and A. G. Wintle (1981). The use of alpha scintillation counting for measuring th-230 and Pa-231 contents of ocean sediments, *Can. J. Earth Sci.* **18**, 419–432.

Khromovskikh, V. S. (1989). Determination of magnitudes of ancient earthquakes from dimensions of observed seismodislocations, *Tectonophysics* **166**, 1–12.

Lamothe, M. (1984). Apparent thermoluminescence ages of St. Pierre sediments at Pierreville, Quebec and the problem of anomalous fading, *Can. J. Earth Sci.* **21**, 1406–1409.

Mabey, D. R. (1985). Geophysical maps of the Mount Naomi Roadless Area, Cache County, Utah and Franklin County, Idaho, U.S. Geol. Surv. Map MF-15661-C, scale 1:100,000.

Machette, M. N., S. F. Personius, and A. R. Nelson (1987). Quaternary geology along the Wasatch fault zone: segmentation, recent investigations, and preliminary conclusions, *U.S. Geol. Surv. Open-File Rep. 87-585*, A1–A72.

Machette, M. N., S. F. Personius, A. R. Nelson, D. P. Schwartz, and W. R. Lund (1989). Segmentation models and Holocene movement history of the Wasatch fault zone, Utah, *U.S. Geol. Surv. Open-File Rep. 89-0315*, 229-245.

McCalpin, J. (1987a). Late Quaternary tectonics and earthquake hazard in Cache Valley, Utah, Final Technical Report, U.S. Geol. Surv. Contract 14-08-0001-G1091, 187 pp.

McCalpin, J. (1987b). Geologic criteria for recognition of individual paleoseismic events in extensional environments, *U.S. Geol. Surv. Open-File Rep. 87-673*, 102-114.

McCalpin, J. (1987c). Recommended setback distances from active normal faults, in *Proc. 23rd Symp. Engineering Geology and Soils Engineering*, J. McCalpin (Editor), Logan, Utah, 306-322.

McCalpin, J. (1989). Surficial geologic map of the East Cache fault zone, Cache County, Utah, U.S. Geol. Surv. Misc. Field Investigations Map MF-2107, scale 1:50,000.

McCalpin, J., L. Zhang, and V. S. Khromovskikh (1990a). Quaternary faulting in the Bear Lake graben, Idaho and Utah, *Geol. Soc. Am. Abstr. Prog.* **22**, No. 5, 38.

McCalpin, J., L. A. Piety, and M. H. Anders (1990b). Latest Quaternary faulting and structural evolution of Star Valley, Wyoming, in *Geologic Field Tours of Western Wyoming and Parts of adjacent Idaho, Montana and Utah*, S. Roberts (Editor), Geological Survey of Wyoming, Public Information circular No. **29**, 5-14.

Nelson, A. R. (1988). The northern part of the Weber segment of the Wasatch fault zone near Ogden, Utah, in *In the Footsteps of G. K. Gilbert: Lake Bonneville and Neotectonics of the Eastern Basin and Range Province*, M. N. Machette (Editor), *Utah Geol. and Min. Survey Misc. Publ.*, **88-1**, 33-37.

Nelson, A. R. and J. T. Sullivan (1987). Late Quaternary history of the James Peak fault, southernmost Cache Valley, north-central Utah, *U.S. Geol. Surv. Open-File Rep. 87-585*, vol. 1, J1-J39.

Ostenaa, D. A. (1984). Relationships affecting estimates of surface fault displacements based on scarp-derived colluvial deposits, *Geol. Soc. Am. Abstr. Prog.* **16**, No. 5, 327.

Personius, S. F. (1988). Preliminary surficial geologic map of the Brigham City segment and adjacent parts of the Weber and Collinston segments, Wasatch fault zone, Box Elder and Weber counties, Utah, U.S. Geol. Surv. Map MF-2042, scale 1:50,000.

Piety, L. A., C. K. Wood, J. D. Gilbert, J. T. Sullivan, and M. H. Anders (1986). Seismotectonic study for Palisades Dam and Reservoir, Palisades Project, *U.S. Bureau of Reclamation Seismotectonic Report 86-3*, 198 pp. and Appendices.

Rendell, H. M. and P. D. Townsend (1988). Thermoluminescence dating of a 10 m loess profile in Pakistan, *Quaternary Sci. Rev.* **7**, 251-255.

Robertson, G. C., III (1978). Surficial deposits and geologic history, northern Bear Lake Valley, Idaho, *M.S. Thesis*, Utah State University, Logan, Utah, 162 pp.

Scott, W. E., W. D. McCoy, R. R. Shroba, and M. Rubin (1983). Reinterpretation of the exposed record of the last two lake cycles of Lake Bonneville, western United States, *Quaternary Research* **20**, 261-285.

Shroba, R. R. (1980). Influence of parent material, climate, and time on soils formed on Bonneville shoreline and younger deposits near Salt Lake City and Ogden, Utah, *Geol. Soc. Am. Abstr. Prog.* **12**, No. 6, 304.

Slemmons, D. B. (1982). Determination of design earthquake magnitudes for microzonation, *Proc. 3rd Intl. Earthquake Microzonation Conference*, **1**, 119-130, Seattle, Washington.

Smith, R. B. and R. L. Bruhn (1984). Intraplate extensional tectonics of the eastern Basin-Range: inferences on structural style from seismic reflection data, regional tectonics, and thermal-mechanical models of brittle-ductile deformation, *J. Geophys. Res.* **89**, 5733-5762.

Soil Survey Staff (1975). *Soil Taxonomy*, U.S. Dept. of Agriculture, Soil Conserv. Service, Agricultural Handbook no. 436, 754 pp.

Swan, F. H., III, K. L. Hanson, D. P. Schwartz, and J. H. Black (1983). Study of earthquake recurrence intervals on the Wasatch fault, Utah, Eighth Semi-Annual Technical Report, U.S. Geol. Surv. Contract No. 14-08-0001-19842, 20 pp.

Wallace, R. E. (1984). Faulting related to the 1915 earthquakes in Pleasant Valley, Nevada, *U.S. Geol. Surv. Profess. Pap.* 1274-A, 33 pp.

Wheeler, R. B. and K. B. Krystinik (1988). Segmentation of the Wasatch fault zone, Utah: summaries, analyses, and interpretations of geophysical data, *U.S. Geol. Surv. Bull.* **1827**, 47 pp.

Wintle, A. G. (1973). Anomalous fading of thermoluminescence in mineral samples, *Nature* **245**, 143-144.

Wintle, A. G. (1985). Sensitization of TL signal by exposure to light, *Ancient TL* **3**, 11-13.

Wintle, A. G. (1973). Anomalous fading of thermoluminescence in mineral samples, *Nature* **245**, 143–144.

Wintle, A. G. (1985). Sensitization of TL signal by exposure to light, *Ancient TL* **3**, 11–13.

Wintle, A. G. and D. J. Huntley (1982). Thermoluminescence dating of sediments, *Quaternary Sci. Rev.* **1**, 31–53.

Zoback, M. L. (1983). Structure and Cenozoic tectonism along the Wasatch fault zone, Utah, *Geol. Soc. Am. Mem.* **157**, 3–27.

Appendix 1

A majority of sediments sampled in the Logan trench were compact silty sands and required large and sturdy containers for TL sampling. Steel soup cans (8 cm diameter by 10 cm long) with the outer edge serrated using metal snips were "augered" into the section and were an effective vessel for retrieving a large volume of sediment protected from sunlight exposure. After sampling, the open end of the can was covered immediately with aluminum foil, and secured with duct tape. Cans were then stored in black plastic bags before being shipped to the laboratory for TL analysis.

Appendix 2

Thermoluminescence dating analyses were performed on 14 samples by Alpha Analytic, Inc., Coral Gables, Florida. Alpha Analytic determined EDs for all samples by the regeneration, total, and partial bleach techniques (Table 2; see Forman, 1989, for a discussion of these techniques). Linear regression statistics were used to define additive dose functions and an 18-hour exposure to ultraviolet light was used to define the residual level for the total bleach and regeneration techniques. Equivalent dose by the partial bleach method was determined by two procedures, a filtered 18-hour exposure that simulates short subaerial exposure to direct sunlight and a 45-minute exposure to simulate shallow subaqueous exposure (details given in Table 2).

Dose rate of the samples was evaluated from the uranium, thorium and potassium content of the samples (Table 3). Uranium and thorium levels of samples, assuming secular equilibrium, were determined by thick source alpha counting (Huntley and Wintle, 1981). Samples were counted under sealed and unsealed conditions to evaluate the extent of radon loss; most samples exhibited little (< 5 per cent) or no loss of radon. Potassium-40 levels were determined on a separate split of the sample using atomic absorption spectrophotometry to measure the percentage of potassium.

Department of Geology
Utah State University
Logan, Utah 84322-4505
(J.M.C.)

Center for Geochronological Research
INSTAAR
University of Colorado
Boulder, Colorado 80309-0450
(S.L.F.)

Manuscript received 6 June 1989